Journal of Applied Mechanics and Technical Physics, Vol. 42, No. 2, pp. 243–254, 2001

EVOLUTION OF VORTEX STRUCTURES ON THE LEEWARD SIDE OF A DELTA WING

M. D. Brodetsky,[1] E. Krause,[2] S. B. Nikiforov,[1] A. A. Pavlov,[1] A. M. Kharitonov,[1] and A. M. Shevchenko[1]

UDC 533.06

Results of an experimental study of a supersonic flow around the leeward side of a delta wing are presented. The experiments are performed on three delta wings with leading-edge sweep angles $\chi = 68°$, 73°, and 78° for Mach numbers $M = 2$–4 and angles of attack $\alpha = 0$–22°. Data on the structure and position of internal shock waves are obtained; the size and location of primary and secondary vortices are found. New regimes of the flow around a delta wing are identified. The chart of flow regimes around delta wings is refined and extended.

1. At supersonic velocities, there may be various flow regimes on the leeward side of delta wings, which differ by the number and positions of streamwise vortices, internal shock waves, and other features of the flow. Convergence and divergence lines are formed on the upper surface of the wing as a result of flow separation and reattachment. Peaks of heat fluxes arise in reattachment regions with increasing flight velocity. Under certain conditions, flow separation may cause a shift of the center of pressure and a change in the moment characteristics of the wing. In addition, a pair of vortices and internal shock waves may have an adverse effect on the flow around the elements of the flying vehicle located downstream of the delta wing.

These effects make actual the study of the regular features of reconstruction of the spatial flow structure at the leeward side of delta wings to derive a reliable chart of flow regimes in order to predict the appearance of these or those features of the flow depending on the free-stream parameters and wing geometry.

Stanbrook and Squire [1] and Squire [2] proposed to use the normal angle of attack α_N and the normal Mach number M_N as parameters governing the flow topology. These parameters are calculated by the projection of the velocity vector onto the plane normal to the leading edge of the wing (Fig. 1a):

$$\alpha_N = \arctan\,(\tan\,\alpha/\cos\chi), \qquad M_N = M\cos\chi(1+\sin\alpha\tan\,\chi)^{1/2}.$$

Here α is the angle of attack and χ is the sweep angle of the leading edge of the wing. Stanbrook and Squire [1] and Squire [2] identified three main classes of flows (flows with leading-edge separation, flows without leading-edge separation but a detached shock wave, and flows without leading-edge separation but with an attached shock wave) and obtained conditions of their origination. Maikapar [3] observed 13 flow regimes using laser-sheet visualization. Wood and Miller [4] found seven flow regimes in the α_N–M_N coordinates; these regions corresponds to different flows on the leeward side of the wing with different positions and number of internal shock waves and vortices. Szodruch and Peake [5] suggested a chart with a similar classification for thick wings. Seshadri and Narayan [6] proposed another classification, which, on the one hand, supplements the chart proposed in [4] and, on the other hand, does not contain some regimes identified in that paper. Evolution of test equipment allowed one to find new regimes of the flow around a delta wing. In particular, Vorropoulos

[1]Institute of Theoretical and Applied Mechanics, Siberian Division, Russian Academy of Sciences, Novosibirsk 630090. [2]Aachen Institute of Aerodynamics, Aachen 52062, Germany. Translated from Prikladnaya Mekhanika i Tekhnicheskaya Fizika, Vol. 42, No. 2, pp. 68–80, March–April, 2001. Original article submitted April 24, 2000.

0021-8944/01/4202-0243 $25.00

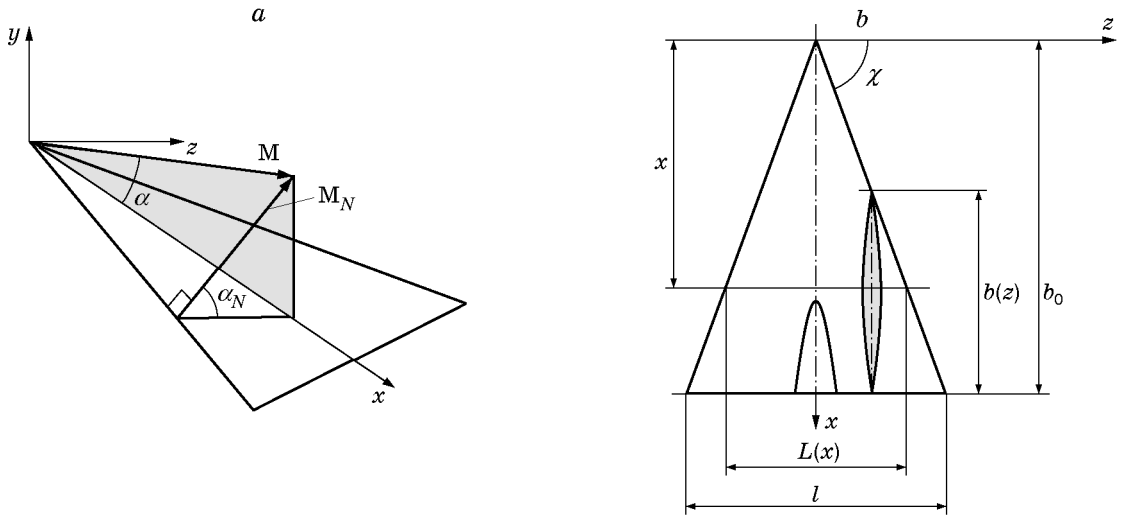

Fig. 1. Schematic of the model and coordinate system: (a) determination of the normal angle of attack α_N and normal Mach number M_N [1]; (b) wing model.

and Wendt [7] experimentally found a new flow regime on the leeward side of a delta wing: the flow with the formation of a shock wave under the primary vortex. By exploring the flow field by multichannel pressure probes and laser-sheet visualization of the flow, Brodetsky and Shevchenko [8] confirmed the existence of this flow regime and found regimes, where this shock wave is observed simultaneously with internal shock waves above and between the pair of primary vortices on the leeward side of the wing. The flow regimes mentioned were observed for the same values of the normal angles of attack and Mach numbers as in [4], though the initial angles of attack, sweep angles, and Mach numbers in these experiments were different.

Thus, until now there is no chart of flow regimes around delta wings, which would allow an unambiguous prediction of flow topology.

In the present paper, we analyze the results of experimental studies of delta wings with sweep angles $\chi = 68°$, 73°, and 78° within the range of Mach numbers M = 2–4 and angles of attack $\alpha = 0$–22°. The test conditions ensured flow regimes around delta wings with a smooth transition from a subsonic to supersonic leading edge and a corresponding reconstruction of the flow with the formation of primary, secondary, and tertiary vortices and internal shock waves.

2. The experiments were performed on a delta-wing model with sharp leading and trailing edges, which is schematically shown in Fig. 1b. Three wings with leading-edge sweep angles $\chi = 68$, 73, and 78° were studied; the lengths of the root chord b_0 were 383, 439, and 526 mm, respectively. All three wings had 3-% symmetric parabolic profiles. The coordinates of the upper (lower) surface were found by the formula

$$y = \pm 2\bar{c}\Big(\bar{x} - \frac{2z}{L}\Big)\frac{1-\bar{x}}{1-2z/L}\,b_0.$$

Here $\bar{c} = c/b(z) = 0.03$ is the maximum relative thickness of the wing profile [c is the maximum thickness of the profile in the cross section $z = \text{const}$ and $b(z)$ is the local chord of the wing], $\bar{x} = x/b_0$, and L is the wing span.

The pressure on the model surface was measured using hanging pipelines [9]. The pressure taps were made with a step of 3 mm in five cross sections perpendicular to the longitudinal axis of the model on wings with $\chi = 68°$ and 73° and in six cross sections on the wing with $\chi = 78°$.

The experiments were conducted in a T-313 supersonic blowdown wind tunnel based at the Institute of Theoretical and Applied Mechanics of the Siberian Division of the Russian Academy of Sciences with a Mach range between 1.75 and 6 [10].

In the experiments, the model was mounted in an arc-shaped suspension of the AV-313M mechanical aerodynamic balance. The error in the angle of attack of the model was ±0.1°.

The experiments were performed for angles of attack of the model $\alpha = 0$–22°, Mach numbers M = 2–4, and the corresponding unit Reynolds numbers $\mathrm{Re}_1 = 26 \cdot 10^6$–$56 \cdot 10^6$ m^{-1}.

The test conditions allowed us

— to cover the greatest possible range of α_N and M_N with the formation of primary and secondary vortices on the leeward side of the wing and internal shock waves above and under the primary vortex;

— to obtain experimental data on wings with different sweep angles for different angles of attack but close values of α_N and M_N.

The test techniques included visualization of the limiting streamlines, static-pressure measurement on the model surface, and also visualization of the spatial flow pattern by the laser-sheet technique. Visualization of the limiting streamlines was also performed by the method of oil–soot coatings.

The pressure on the model surface was measured by a MID-100 multichannel pressure meter [11]. The range of the measured pressure was 0–10^5 Pa, and the instrumental error was less than 0.3% of the upper limit of pressure measurement. The measurement results were used to determine the pressure coefficients $C_P = (P - P_\infty)/q$, where P is the static pressure on the model surface, P_∞ is the free-stream static pressure, and q is the dynamic pressure. The spatial flow pattern was visualized by the laser-sheet technique described in [12].

3. The main features of the flow on the leeward side of the wing within a wide range of α_N for $\mathrm{M}_N < 0.8$ are the vortex sheet shed from the sharp leading edges of the wing, which rolls up into a pair of primary vortices with a possible appearance of internal shock waves above, under, and between them. Figure 2 shows the test results for the wing with $\chi = 78^\circ$ for M = 2 and $\alpha = 14^\circ$. Separating from the leading edges (convergence line S_1), the flow reattaches along the line A_1, which is a divergence line. Flow reattachment leads to a local pressure increase at the point of reattachment. A low-pressure region is formed under the primary vortex. The minimum value of pressure is determined by the spanwise position of the core of the primary vortex (Fig. 2d). With increasing angle of attack, the strength of the primary vortex increases, causing a further decrease in pressure on the leeward side of the wing. The adverse pressure gradient (pressure increase between its minimum and the leading edge) may be sufficient to force boundary-layer separation along the convergence line S_2. Secondary separation of the flow (secondary vortex) arises. It reattaches again along the divergence line A_2. For higher angles of attack, tertiary separation along the convergence line S_3 may appear inside the region of secondary separation, with reattachment along the divergence line A_3. Secondary separation has a much smaller effect on the pressure distribution over the wing surface. The local pressure minimum under the secondary vortex and the pressure maximum corresponding to the reattachment line A_2 are usually expressed rather weakly. Tertiary separation has almost no effect on the pressure distribution over the wing surface. It is usually identified only by the pattern of the limiting streamlines on the model surface.

We consider the main topological features of the flow and the effect of the angles of attack and sweep and the Mach number on the flow structure.

Figure 3 shows the pictures obtained by laser-sheet visualization of the flow in the plane perpendicular to the model centerline on the wing with $\chi = 78^\circ$. In Fig. 3a (M = 2.75 and $\alpha = 16^\circ$), one can see a part of the model between the laser-sheet plane and the trailing edge, the bow shock wave, the vortex sheet induced by the leading edges, which rolls up into the primary vortex, and also the region of secondary separation, the internal shock wave above the primary vortex, the internal shock wave under the primary vortex, and λ-shaped wave structures above the vortex sheet and the primary vortex, which were not observed previously.

Figure 4 shows the surface streamlines obtained by the method of oil–soot coatings on the wing with $\chi = 78^\circ$ for M = 2. Figure 4a–c shows the pictures obtained on different halves of the wing in different experiments with two angles of attack. The origination of primary separation of the flow on sharp leading edges was observed on the wing with $\chi = 78^\circ$ already for $\alpha = 2^\circ$ ($\alpha_N = 9.5^\circ$). This was evidenced by the appearance of the divergence line A_1 along which the flow separated from the sharp leading edges was reattached to the leeward side of the wing (Fig. 4a). On laser-sheet patterns of the flow, a small vortex is observed only for M = 2 (see Fig. 3b). It was not observed for higher Mach numbers (M = 2.5–4) and $\alpha = 2^\circ$. At the same time, the divergence line A_1 was observed on the wing surface (Fig. 4a). Beginning from $\alpha = 4^\circ$, an onset of separation on sharp leading edges was observed for all examined values of χ and M corresponding

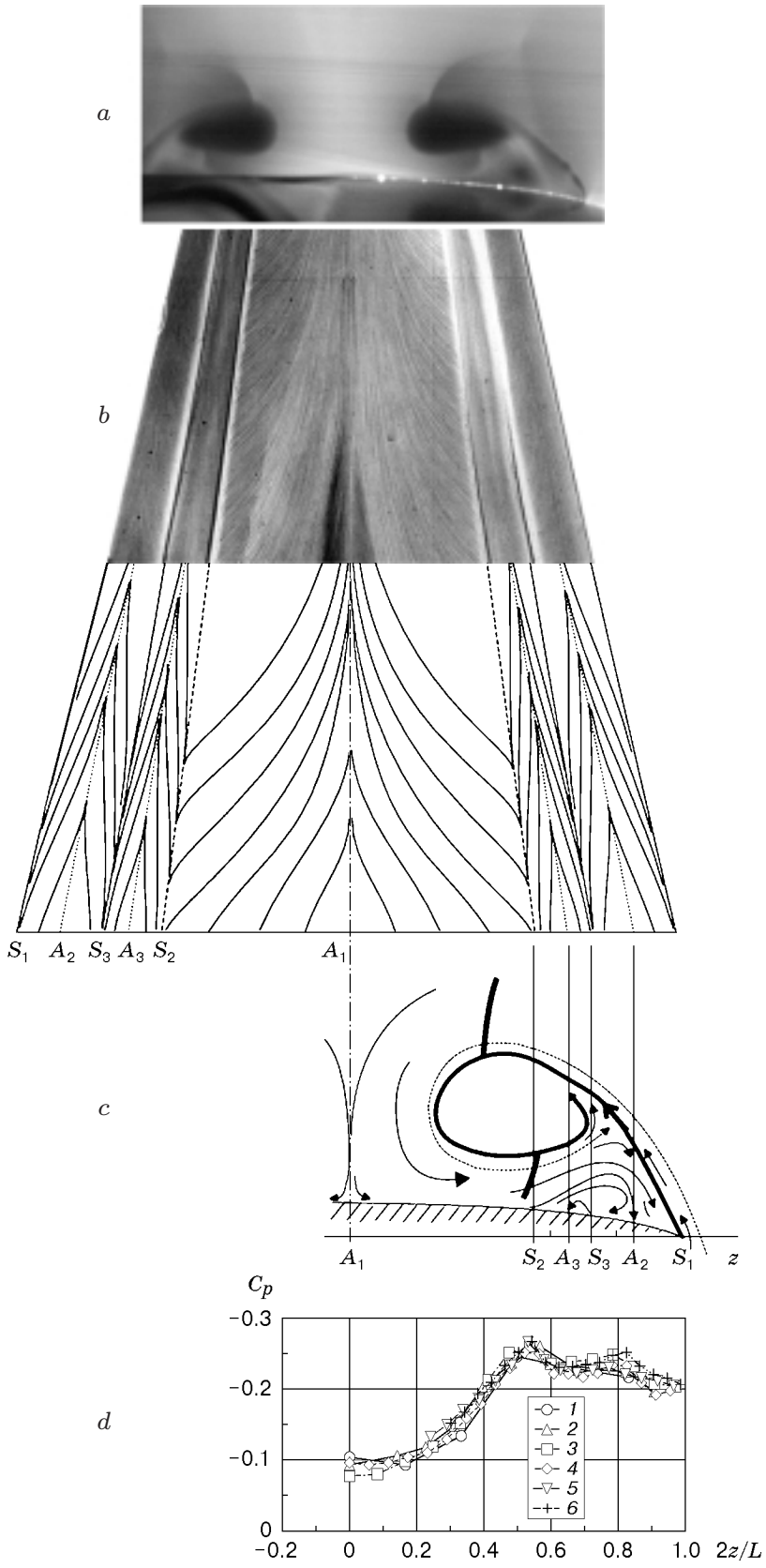

Fig. 2. Flow features on the leeward side of a delta wing with $\chi = 78°$ for M = 2 and $\alpha = 14°$: (a) laser-sheet visualization; (b) oil–soot visualization of the limiting streamlines and topological scheme of the flow on the wing surface; (c) flow topology on the leeward side of the wing; (d) static-pressure distribution on the leeward side of the wing for $x/b_0 = 0.162$ (1) 0.316 (2), 0.433 (3), 0.618 (4), 0.741 (5), and 0.890 (6).

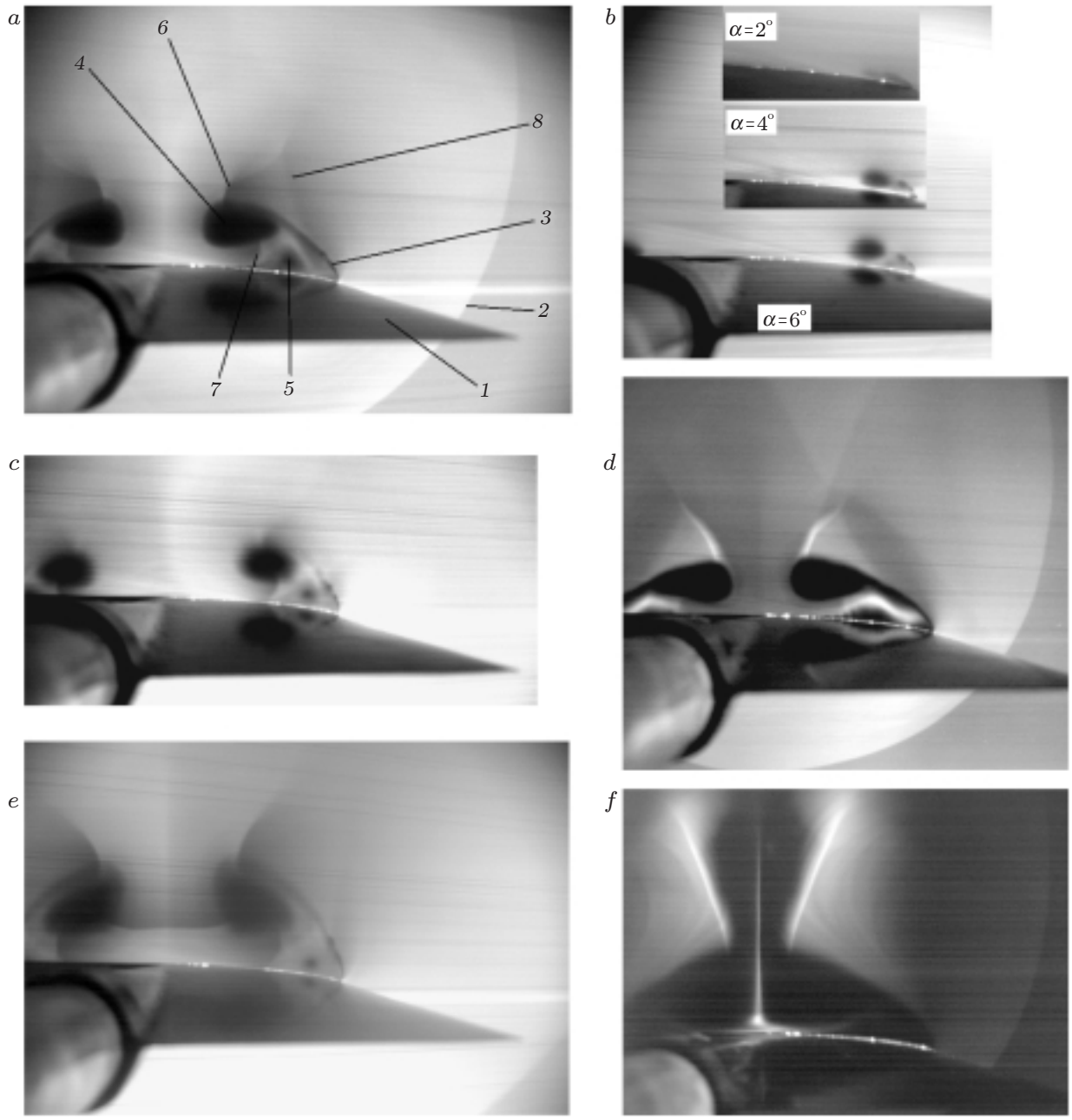

Fig. 3. Laser-sheet visualization on the wing with $\chi = 78^\circ$ for M = 2.75 and $\alpha = 16^\circ$(a), M = 2 and $\alpha = 2$–6°(b), M = 2 and $\alpha = 12^\circ$(c), M = 3.5 and $\alpha = 16^\circ$(d), M = 2 and $\alpha = 22^\circ$ (e), and M = 4 and $\alpha = 22^\circ$ (f): 1) trailing edge of the wing; 2) bow shock wave; 3) vortex sheet; 4) primary vortex; 5) secondary separation; 6) internal shock wave above the primary vortex; 7) internal shock wave under the primary vortex; 8) λ-shaped wave structure.

to $M_N < 0.8$. It should be noted that the flow is not conical for small angles of attack. The line A_1 (Fig. 4a) begins not from the wing tip but from the leading edge at a certain angle to the root chord of the wing.

With increasing angle of attack, the strength of the primary vortex increases. This is accompanied by an increase in circular velocities at the periphery of the vortex core and by a drastic decrease in gas density in the core of the compressed vortex. An increase in velocity leads to an increase in separation of light-scattering particles from the vortex core, and a decrease in density leads to a decrease in concentration of these particles.

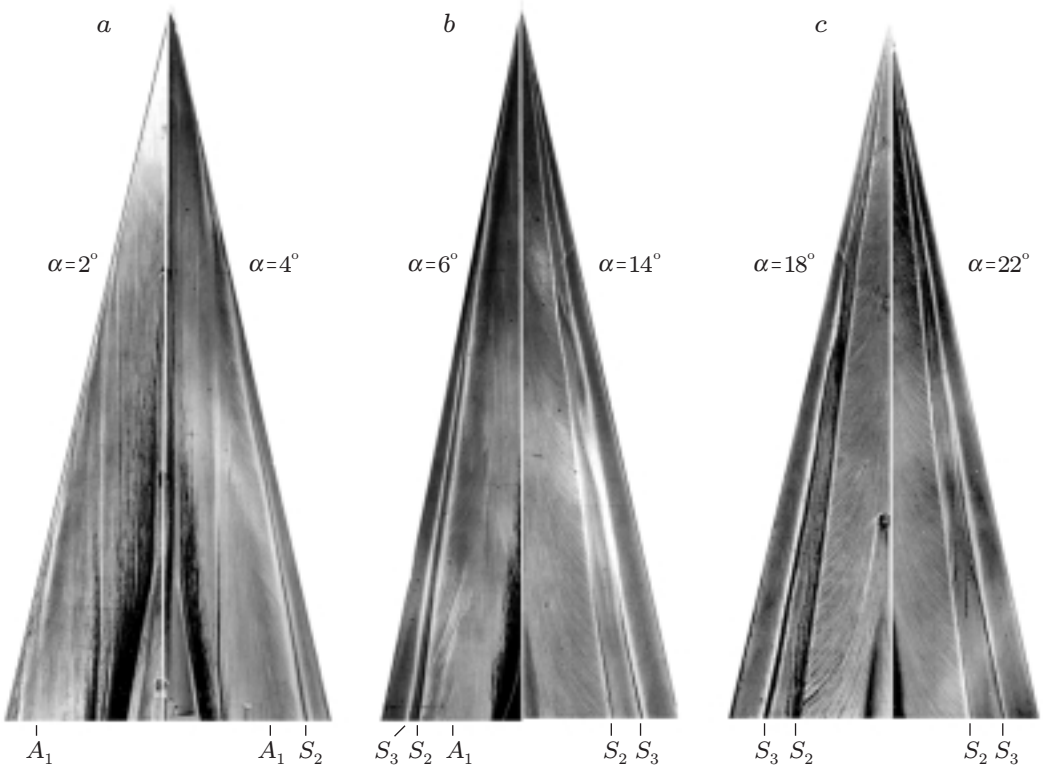

Fig. 4. Visualization of the limiting streamlines ($\chi = 78^\circ$ and M = 2) for $\alpha = 2^\circ$ and 4° (a), 6° and 14° (b), and 18° and 22° (c).

Therefore, the vortex core has a greater contrast in the images shown in Fig. 3c and d. With increasing angle of attack, the vortex core increases in size and moves farther from the model surface. Internal shock waves arise in the vicinity of the vortex core (the wave structure is considered below). The distance between the cores of the primary vortices decreases (see also Fig. 6). The vortex sheet and the core of the primary vortex occupy a greater and greater area above the leeward side of the wing. The same evolution of the pair of primary vortices with increasing α was observed within the entire examined range of Mach numbers corresponding to $M_N < 1$.

With increasing Mach number for a fixed value of α, the core of the primary vortex becomes flatter, it approaches the wing and occupies a large area above its surface. The vortex core has more distinct boundaries. The distance between the vortex cores decreases with increasing Mach number (cf. Fig. 3a and Fig. 3d; Fig. 3e and Fig. 3f). For M = 4, vortex cores almost merge with each other, and a vortex-street flow is formed above the pair of primary vortices between the shock waves (see Fig. 3f).

The adverse pressure gradient is sufficient for boundary-layer separation and emergence of a secondary-separation region. This is evidenced by the appearance of the convergence line S_2 at $\alpha = 4^\circ$ with flow separation from the wing surface along this line (see Fig. 4a). The divergence line A_2 appears near the leading edge; reattachment of secondary separation occurs along this line. Based on the laser-sheet pictures, the secondary separation is unambiguously recognized for $\alpha > 6^\circ$, where the core of the primary vortex moves away from the wing surface (see Fig. 3b).

It follows from visualization of the limiting streamlines that tertiary separation arises on the wing surface in certain flow regimes. The area of this separation is so small that it is normally determined only in the pattern of the limiting streamlines, in particular, by the appearance of the tertiary-separation line S_3 (see Fig. 4b and c). This separation is not visible in laser-sheet images and exerts practically no effect on the pressure distribution over the wing surface. Obviously, the secondary-separation region should be rather

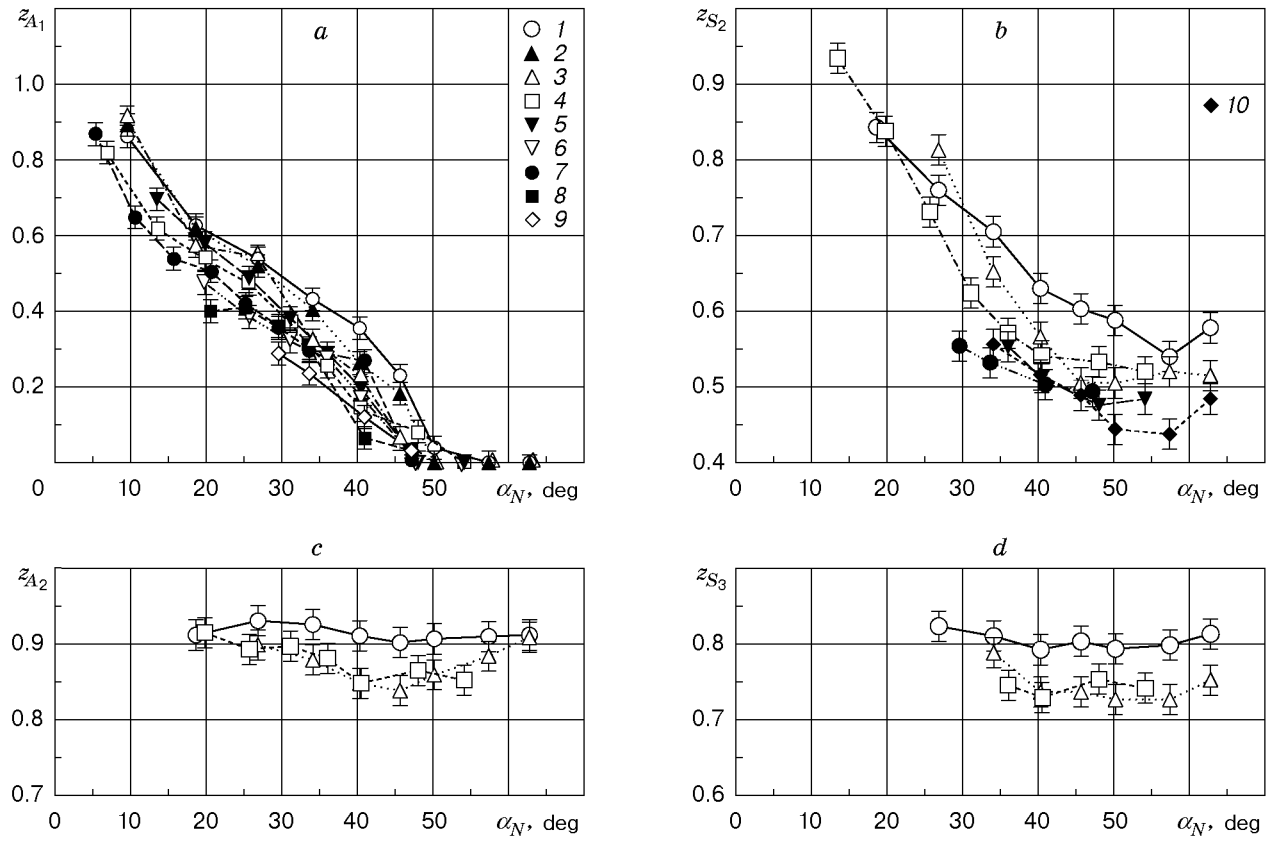

Fig. 5. Positions of the lines of reattachment of primary separation z_{A_1} (a), secondary separation z_{S_2} (b), reattachment of secondary separation z_{A_2} (c), and tertiary separation z_{S_3} (d) versus the normal angle of attack for $\chi = 78^\circ$ and M = 2 (1), $\chi = 78^\circ$ and M = 2.5 (2), $\chi = 78^\circ$ and M = 2.75 (3), $\chi = 73^\circ$ and M = 2 (4), $\chi = 73^\circ$ and M = 2.5 (5), $\chi = 73^\circ$ and M = 3 (6), $\chi = 68^\circ$ and M = 2 (7), $\chi = 68^\circ$ and M = 2.25 (8), $\chi = 68^\circ$ and M = 2.5 (9), and $\chi = 78mm^\circ$ and M = 3.5 (10).

developed for tertiary separation to appear. In the present study, the minimum values of the normal angle of attack and Mach number for which tertiary separation was observed were $\alpha_N = 26.8^\circ$ and $M_N = 0.47$; these values were obtained on the wing with $\chi = 78^\circ$ for $\alpha = 6^\circ$ and M = 2. It is seen in Fig. 4b that the convergence line S_3 appears under these conditions, which indicates the formation of tertiary separation under the secondary vortex. For high Mach numbers, tertiary separation occurs later. Thus, for the same wing, the line of tertiary separation S_3 was observed for angles of attack $\alpha \geqslant 8^\circ$ at M = 2.5 and M = 2.75 and for $\alpha \geqslant 10^\circ$ at M = 3. The data for the wing with $\chi = 73^\circ$ show that, for M = 2, tertiary separation appears for the first time for $\alpha = 8^\circ$, which corresponds to $\alpha_N = 25.7^\circ$ and $M_N = 0.65$. The line S_3 begins not from the wing tip but branches off from the line S_2 at a certain distance from the wing tip. Similar patterns of the limiting streamlines were obtained for $\alpha = 10$ and 12°. For $\alpha = 14$–22°, the line S_3 was observed (as in the case with $\chi = 78^\circ$) along the entire wing beginning from its tip. With increasing angle of attack, the distance between the lines S_2 and S_3 increases (see Fig. 4b and c).

Figure 5 shows the relative coordinates of the point of intersection of separation and reattachment lines with the line $x = \text{const}$ versus the normal angle of attack. The data were obtained by processing the results of visualization of the limiting streamlines. The flow was assumed to be conical, and all the coordinates of separation and reattachment lines were normalized to the local half-span of the wing. The uncertainty bars are shown in the figures. It is seen in Fig. 5a that the position of the reattachment line A_1 is mainly determined by the angle of attack of the wing. With increasing the latter, the line A_1 is shifted from the leading edge to the center, and, for $\alpha_N > 50^\circ$, the reattachment of primary separation occurs on the axis of symmetry of the wing. It should be noted that the position of the line A_1 depends weakly on the Mach number within

the range from 2 to 2.75. For low angles of attack, the sweep angle of the wing has almost no effect on the position of the reattachment line A_1.

It is shown in Fig. 5b that the position of the secondary-separation line depends on the angle of attack only for its low and moderate values (up to $\alpha = 12°$, i.e., $\alpha_N = 40$–$45°$). With increasing angle of attack, the region of secondary separation increases, and the line S_2 is shifted from the wing edge to its central part. For $\alpha_N > 35°$, its position remains almost unchanged. This line is located at a distance of 45–55% of the local half-span of the wing from the root cross section of the wing. Good agreement in the values of z_{S_2} for $\alpha_N > 35°$ for wings with different sweep angles should be noted for different Mach numbers but close values of α_N and M_N (cf. curves 5, 7, and 10 and also curves 3 and 4 in Fig. 5b).

Figure 5c shows the relative coordinates of the point of intersection of the reattachment line of secondary separation A_2 with the line $x = \text{const}$ versus the normal angle of attack. They are almost independent of the angle of attack and weakly depend on the Mach number (for the wing with $\chi = 78°$). For all three regimes considered, the line A_2 is located near the leading edge (at a distance equal to 10–15% of the local half-span of the wing). Good agreement of data obtained for two different wings (curves 3 and 4 in Fig. 5c) but identical α_N and M_N should be noted.

It follows from Fig. 5d that the position of the tertiary-separation line is independent of the angle of attack. For $\chi = 78°$ and $M = 2$ (curve 1), it is located at a distance of 80% of the local half-span of the wing from its root cross section. With increasing Mach number to 2.75 or with decreasing sweep angle, the line S_3 is shifted by 5–7% toward the root cross section of the wing. The data for the regimes with $\chi = 78°$ and $M = 2.75$ (curve 3) and $\chi = 73°$ and $M = 2$ (curve 4) are in good agreement.

For high angles of attack, the flow above the pair of primary vortices and the vortex sheet becomes conically supersonic (the projection of the velocity vector onto the plane perpendicular to the ray emanating from the wing tip is greater than the velocity of sound). The axial rotation of two conically supersonic flows directed from the leading edges of the wing to the plane of the central symmetry toward each other gives rise to internal shock waves above the pair of primary vortices. In Wood and Miller's diagram [4], these regimes correspond to the region above boundary II (Fig. 7). The region of flow regimes around the wing without the formation of these internal shock waves lies beneath this boundary. However, it follows from the results of the present work that this boundary is not uniquely determined. For $\alpha = 2$–$6°$, no internal shock waves are observed. For $\alpha = 8°$, weak shock waves are seen in laser-sheet pictures: one shock wave above the vortex sheet and two shock waves above the primary vortex (Fig. 6a). For $\alpha = 10°$, a λ-structure is formed above the vortex sheet (Fig. 6b); the shock wave above the primary vortex seems not to be formed yet. With increasing angle of attack, the shock-wave strength increases. The internal stem of the λ-shock moves closer to the vertical plane of symmetry (Fig. 6c). Finally, for $\alpha = 14°$, it is closed on the primary shock wave above the vortex (Fig. 6d). For $M = 2.5$, this closure was observed for $\alpha = 18°$. A further increase in the angle of attack leads to a greater strength of the shock wave above the vortex; it extends upward to a greater distance from the vortex core. The regime with the formation of λ-shaped internal shock waves transforms to the regime of the flow around a delta wing with one shock wave above the primary vortex (Fig. 6e and f). With increasing Mach number, this transition is observed for lower values of the angle of attack of the wing.

For high angles of attack, a shock wave appears between the pair of primary vortices. In the present experiments, it was observed for $\alpha_N > 57°$ ($\chi = 78°$ and $\alpha \geqslant 18°$), which is in good agreement with Wood and Miller's chart of flow regimes [4]. It follows from Fig. 3e and Fig. 6e and f that the shock wave is located approximately at an unchanged stand-off distance from the wing. With increasing angle of attack from 18° ($\alpha_N = 57.4°$) to 22° ($\alpha_N = 62.8°$), its shape changes. For instance, for $\alpha = 18°$, this shock wave is convex upward from the wing surface; for $\alpha = 22°$, vice versa, it is concave downward, to the wing.

As is noted above, with increasing Mach number, the distance between the cores of the primary vortices decreases. For $M = 4$ and $\alpha = 22°$, a regime with merging of vortex cores is observed. It was found that the shock wave between the primary vortices disappears for $\alpha_N > 57°$ and the Mach number changing from 3.5 to 4. This is most likely due to the fact that the strength of the shock wave above the vortex increases. The flow in this shock wave is stronger decelerated and does not have enough time to be accelerated again to a conically supersonic state.

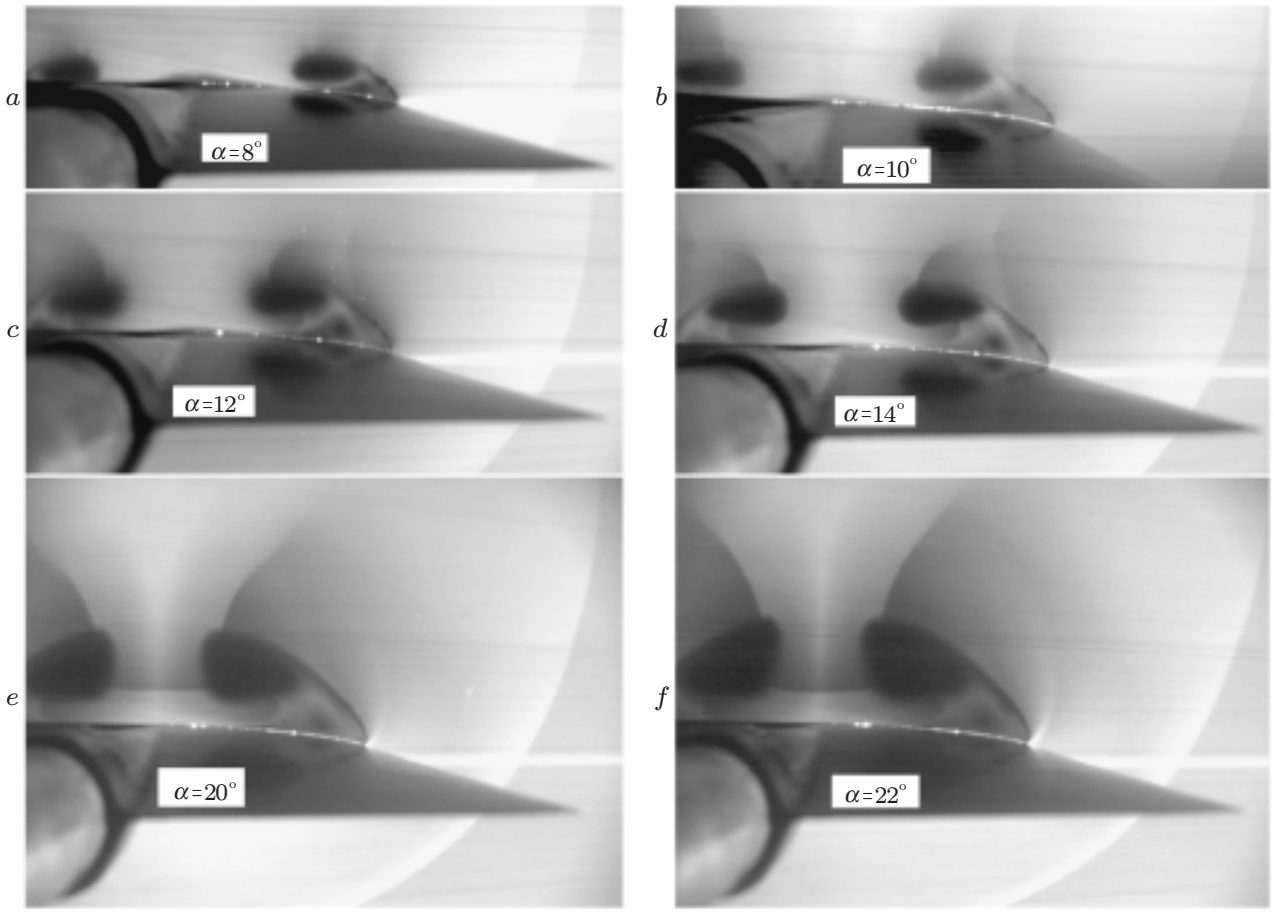

Fig. 6. Laser-sheet visualization of the flow ($\chi = 78°$ and M = 2.75) for $\alpha = 8°$ (a), 10° (b), 12° (c), 14° (d), 20° (e), and 22° (f).

It is shown [8] that Wood and Miller's chart of flow regimes in the α_N–M_N coordinates has a region corresponding to flow regimes around delta wings with the formation of an internal shock wave under the primary vortex (see Fig. 3a, c, and e and Fig. 6). It was also noted in [8] that the appearance or disappearance of this shock wave does not affect (within one regime in Wood and Miller's chart [4]) the appearance or disappearance of other features of the flow regime (secondary separation, shock waves above and between the primary vortices, etc.). The shock-wave formation under the primary vortex seems to be caused by the following reasons. The primary vortex generates high circular velocities at the core periphery. As a result, the flow between the primary vortex and the wing surface becomes conically supersonic. Approaching the leading edge of the wing, it has to turn in the axial direction (along the ray emanating from the wing tip), since the flow near the leading edge forms a kind of an obstacle for it. This deflection of a conically supersonic flow gives rise to a shock wave under the primary vortex. In the present study, the minimum values of the normal angle of attack and Mach number for which this shock wave observed were $\alpha_N = 34°$ and $M_N = 0.5$ ($\chi = 78°$, $\alpha = 8°$, and M = 2). This contradicts the data of [6], according to which this shock should have appeared already for $\alpha_N = 16°$. However, Seshadri and Narayan [6] did not use spatial flow diagnostics and analyzed flow regimes on the basis of visualization of the surface streamlines and pressure measurement on the wing surface, which makes doubtful the results they obtained for the flow topology outside the wing surface.

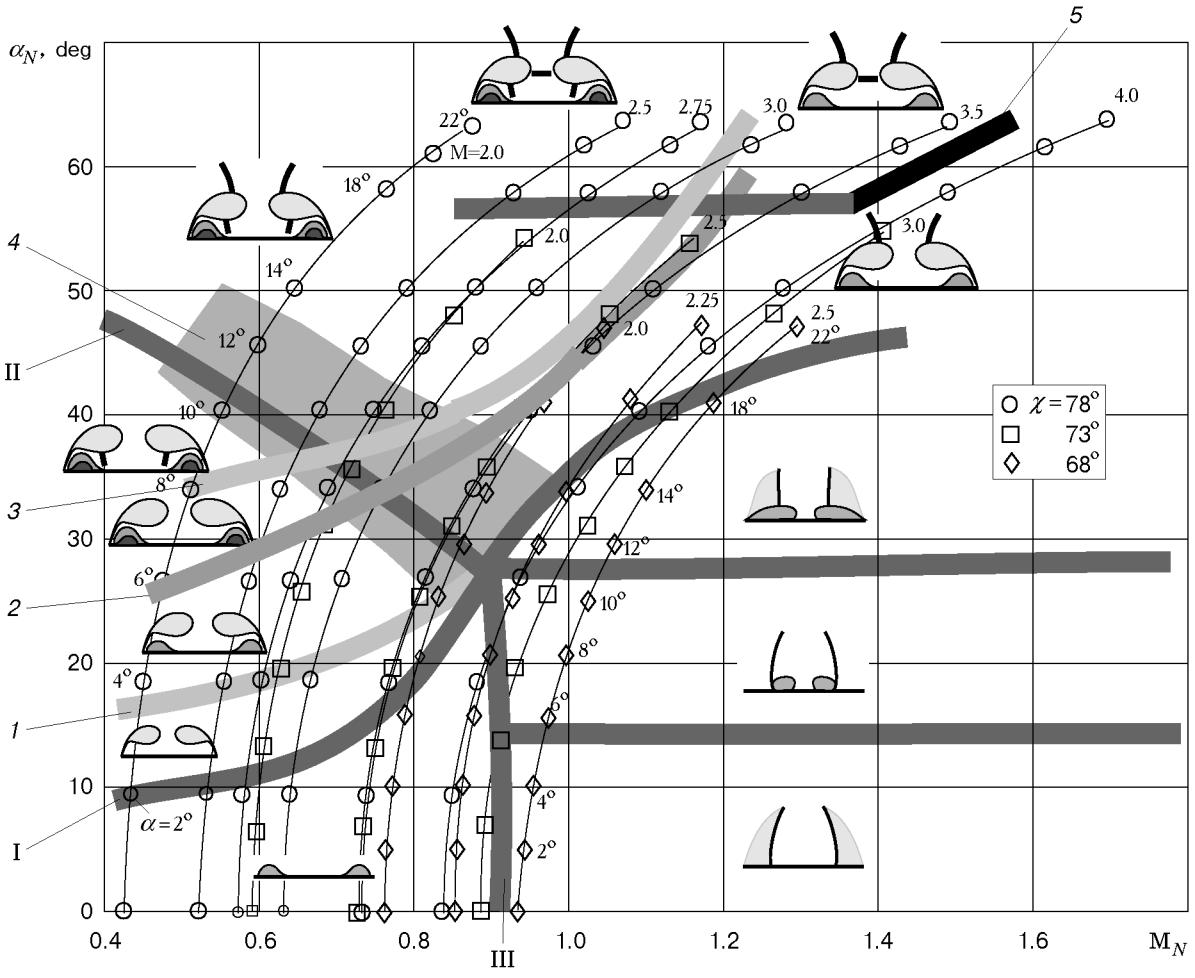

Fig. 7. Chart of flow regimes around the delta wing, where I, II, and III are the boundaries of Wood and Miller's regimes [4], 1 and 2 are the boundary of regimes with secondary and tertiary separation, respectively, 3 is the boundary of regimes with a shock wave under the primary vortex, 4 is the region of transitional regimes, and 5 is the boundary of regimes with a shock wave between the pair of primary vortices.

An analysis of test results allowed us to determine the influence of the Mach number and the angles of attack and sweep on the crossflow topology and add new regions to the known chart of flow regimes around a delta wing (see [4]). Figure 7 shows the Wood and Miller's chart in the M_N–α_N coordinates. The points (M_N, α_N) correspond to flow regimes around a delta wing, which were studied in the present work. The Roman numerals indicate the boundaries of regimes determined in [4], and the Arabic numerals show the boundaries of regimes found in the present study.

An analysis of data obtained within the entire examined range of Mach numbers and angles of attack and sweep of the wing allowed us to draw the boundary of the onset of secondary separation in the chart of flow regimes (curve 1 in Fig. 7). It lies above boundary I in Wood and Miller's chart [4], which separates regimes with and without leading-edge separation. With increasing Mach number, secondary separation appears later, i.e., at higher angles of attack.

The results of analysis of the topology of the streamlines on the wing surface yield boundary 2 dividing regimes of separated flow around the wing with and without tertiary separation. It should be noted that this boundary lies above the boundary obtained in [6]. Based on the data of [6], tertiary separation should appear at $\alpha_N = 16°$. It is seen in Fig. 7 that an increase in the Mach number at high angles of attack leads to the disappearance of tertiary separation.

Curve 3 in Fig. 7 is the boundary of regimes in which a shock wave under the primary vortex was observed. The region of regimes with a shock wave under the primary vortex is to the left of this boundary and above it; the region of regimes without this shock wave is to the right of this boundary and below it. The shock wave is observed simultaneously with other topological features in accordance with Wood and Miller's chart (primary and secondary vortices, the shock above the primary vortex, etc.). As is shown in Fig. 7, the boundary of regimes with a shock wave under the primary vortex is close to the boundary of the onset of tertiary separation. This allows us to assume that the emergence of tertiary separation is related to the shock wave under the primary vortex.

As is noted above, the transition from the regime of the flow around a delta wing without the formation of internal shocks to regimes with shock waves above the primary vortex is smooth rather than jumplike. Transitional regimes correspond to region 4 in Fig. 7.

It follows from the results of visualization of the spatial flow pattern that the shock wave between the pair of primary vortices disappears at $M > 3.5$ for high angles of attack. This transition corresponds to boundary 5. The values of α_N and M_N to the left and right of this boundary correspond to regimes with and without the formation of a shock wave between the primary vortices.

4. Thus, the data on pressure distribution and topology of the surface streamlines on the leeward side of the wing are obtained for three delta wings with sharp leading edges and sweep angles $\chi = 68$, 73, and 78° within the ranges of Mach numbers $M = 2$–4 and angles of attack $\alpha = 0$–22°; the spatial flow structure is visualized.

The present investigations allow us to find a number of special features of the flow around a delta wing. New regimes are observed, which are characterized by a system of weak compression waves above the vortex sheet and the primary vortex, by a λ-shock without the formation of the primary shock wave above the primary vortex, and by a λ-shock with the formation of the primary shock wave above the primary vortex.

An analysis of test results allows us to add the following features to the existing chart of flow regimes around a delta wing: the boundary for the onset of secondary separation, the boundary for the onset of tertiary separation, the boundary of regimes characterized by a shock wave under the primary vortex, the right boundary of regimes with the formation of a shock wave between the pair of primary vortices, and the region of smooth transition from regimes of shock-free flow above the primary vortex to regimes with the formation of this shock wave.

This work was supported by INTAS (Grant No. 96-2358) and the Russian Foundation for Fundamental Research (Grant No. 00-01-00907).

REFERENCES

1. A. Stanbrook and L. C. Squire, "Possible types of flow at swept leading edges," *Aeronaut. Quart.*, **15**, No. 2, 72–82 (1964).
2. L. C. Squire, "Flow regimes over delta wings of supersonic and hypersonic speeds," *Aeronaut. Quart.*, **27**, No. 1, 1–14 (1976).
3. G. I. Maikapar, "Separated flows at the leeward side of a delta wing and a body of revolution in a supersonic flow," *Uch. Zap. TsAGI*, **13**, No. 4, 22–33 (1982).
4. R. M. Wood and D. C. Miller, "Lee side flow over delta wings at supersonic speeds," *J. Aircraft*, **21**, 680–686 (1984).
5. J. G. Szodruch and D. J. Peake, "Leeward flow over delta wings at supersonic speeds," Report NASA TM No. 81187 (1980).
6. S. N. Seshadri and K. Y. Narayan, "Possible types of flow on lee-surface of delta wing at supersonic speeds," *Aeronaut. J.*, No. 5, 185–199 (1988).
7. G. Vorropoulos and J. F. Wendt, "Laser velocimetry study of compressibility effect on the flow field of a delta wing," Report AGARD CP No. 342 (1983).
8. M. D. Brodetsky and A. M. Shevchenko, "Some features of a separated flow and supersonic vortex structure at the leeside of a delta wing," in: *Proc. of the IUTAM Symp. on Separated Flows and Jets* (Novosibirsk, July 9–13, 1990), Springer-Verlag, Berlin–Heidelberg (1991), pp. 341–344.

9. M. D. Brodetsky, S. N. Bruk, and A. M. Makhnin, "Error of determining the pressure coefficients at supersonic velocities," in: *Collected Scientific Papers* [in Russian], Inst. Theor. Appl. Mech., Sib. Div., Acad. of Sciences of the USSR, Novosibirsk (1977), pp. 94–113.
10. I. I. Volonikhin, V. D. Grigor'ev, V. S. Dem'yanenko, et al., "T-313 supersonic wind tunnel," in: *Aerophysical Research* (collected scientific papers) [in Russian], Inst. Theor. Appl. Mech., Sib. Div., Acad. of Sci. of the USSR, Novosibirsk (1972), pp. 8–11.
11. M. A. Amelina, M. D. Brodetsky, I. I. Volonikhin, et al., "MID-100 multichannel pressure meter," in: *Methods and Techniques of Aerophysical Research* (collected scientific papers) [in Russian], Inst. Theor. Appl. Mech., Sib. Div., Acad. of Sci. of the USSR, Novosibirsk (1978), pp. 98–113.
12. L. G. Vasenev, S. B. Nikiforov, A. A. Pavlov, and A. M. Shevchenko, "Development of the laser sheet imaging method for supersonic wind tunnels," in: *Proc. of the 9th Conf. of the Methods of Aerophys. Res.* (Novosibirsk, June 29–July 3, 1998), Part 2, Inst. Theor. Appl. Mech., Sib. Div., Russian Acad. of Sci. (1998), pp. 206–211.